UDC: 662.997

# COMPREHENSIVE INVESTIGATION OF HYDRODYNAMIC PHENOMENA AND FLOW CHARACTERISTICS IN DOMESTIC WATER HEATING SYSTEMS

**Khamraev S.I.**

*Karshi Engineering Economics Institute (PhD., docent), 180100, Karshi, Uzbekistan*

*ORCID ID 0000-0002-0847-9488*

*E-mail : xamrayev@bk.ru*

**Abstract**. The article analyzes the energy consumption for heating a one-story model experimental house, hot water warm floor for experimentation operating at the landfill of alternative energy sources of the Karshi Institute of Engineering and Economics in Kashkadarya region. Based on the analysis, a scheme of the experimental house was created, which will be used in the development of energy saving measures for heating the buildings.

**Key words:** floor, heating, ventilation, indoor air temperature, outside temperature, electricity consumption, natural gas, energy saving. fuel energy, warm floor.

**Аннотация**. В статье анализируется потребление энергии на отопление одноэтажного модельного экспериментального дома, горячего водяного теплого пола для экспериментов, работающего на полигоне альтернативных источников энергии Каршинского инженерно-экономического института в Кашкадарьинской области. На основе проведенного анализа была создана схема экспериментального дома, которая будет использоваться при разработке энергосберегающих мероприятий по отоплению зданий.

**Ключевые слова:** пол, отопление, вентиляция, температура воздуха в помещении, температура наружного воздуха, потребление электроэнергии, природный газ, энергосбережение. топливная энергия, теплый пол.

**Annotatsiya**. Maqolada Qashqadaryo viloyatidagi qarshi muhandislik-Iqtisodiyot institutining muqobil energiya manbalari poligonida ishlaydigan bir qavatli namunaviy tajriba uyini, tajriba o'tkazish uchun issiq suvli issiq polni isitish uchun energiya sarfi tahlil qilinadi. Tahlil asosida binolarni isitish uchun energiya tejash choralarini ishlab chiqishda foydalaniladigan eksperimental uyning sxemasi yaratildi.

**Kalit so'zlar:** zamin, isitish, shamollatish, ichki havo harorati, tashqi harorat, elektr energiyasi iste'moli, tabiiy gaz, energiya tejash. yoqilg'i energiyasi, issiq zamin.

## Introduction

**Description of the Experimental Setup and Research Methodology.** Enhancing the energy efficiency of residential buildings in rural regions,



ISSN 3030-3907

particularly those located far from centralized energy supply networks, while simultaneously reducing the consumption of conventional fuel resources, has become a pressing challenge in recent years [1, 2]. This issue is especially critical during the winter season, when rural households require reliable heating and fuel provision. One of the most effective approaches to addressing this challenge is the application of renewable energy sources [3–6], the development of efficient indoor thermal storage systems [7, 8], and the implementation of hydronic underfloor heating technologies [9, 10, 23–27].

In recent years, water-based underfloor heating systems have gained wide popularity in the construction of single-story residential houses. Initially, these systems were introduced as a supplementary component to conventional heating methods, primarily aimed at enhancing indoor comfort. Their principal advantage lies in the uniform distribution of thermal energy throughout the room. In such systems, the air temperature measured at foot level is typically 3–5 °C higher than that at head level, which corresponds to the most physiologically favorable conditions for human comfort [11].

Compared to traditional radiator-based heating, underfloor systems operate with relatively low temperature gradients between the heating surface and ambient air. This reduces the intensity of convective heat transfer, subsequently lowering indoor airflow velocities. As a result, the circulation of airborne impurities is diminished, while the overall humidity of the indoor environment is maintained at more favorable levels [12].

Underfloor heating systems can generally be classified into two primary categories based on their heat source: electric systems and hydronic (water-based) systems. While electric systems are typically easier and quicker to install, their operational costs are substantially higher due to elevated electricity consumption [13]. Furthermore, electric underfloor systems generate electromagnetic fields during operation, which may pose potential health risks to humans.

Standards for thermal comfort in residential spaces stipulate that the maximum permissible temperature of the floor surface should not exceed 26 °C [14]. Additionally, depending on the type of floor covering material, the optimal surface temperature can be determined following the guidelines presented in [15].

At the “Alternative Energy Sources” educational and research center of the Karshi State Technical University, an experimental study was conducted on a one-story rural dwelling fully powered by solar energy. Within this facility, a water-based underfloor heating system integrated with a solar collector was designed and investigated [16]. The schematic layout of the experimental house, along with the installed hydronic heating system, is presented in Figure 1.1.



ISSN 3030-3907



**Figure 1.1. An overview of the experiment solar house and water heated floor system.**

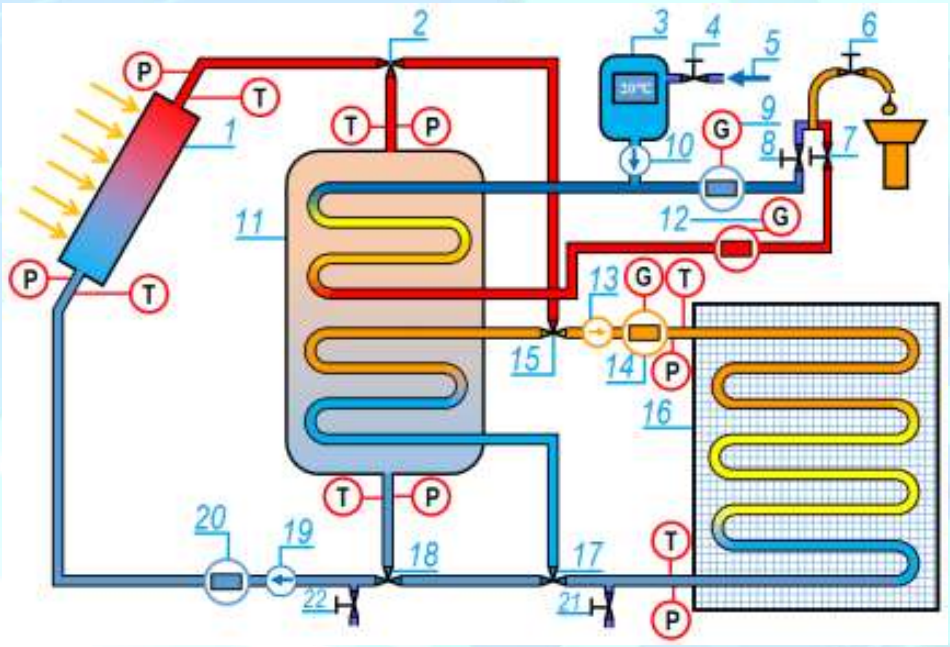
The principal component of the system, along with the fundamental layout of the solar-assisted water-based underfloor heating configuration, is illustrated in Figure 1.2. The proposed design serves multiple research objectives: to examine the performance of underfloor heating systems operating directly on solar energy, to conduct experimental investigations of hydrodynamic and heat transfer processes in water-based heating floors, and to determine the optimal parameters for pipe diameter and installation spacing within the heated floor system.

The solar-collector-assisted hydronic floor heating system is composed of both primary and auxiliary equipment, as outlined below:

a) Flat-plate solar collector — employed to heat the circulating water used in both the underfloor heating system and the storage tank. The collector unit consists of several components: the main casing, embedded water flow pipes, a transparent cover, insulating material, and a set of control and measuring devices designed to monitor water temperature, pressure, and flow rates at both the inlet and outlet of the apparatus. The structural specifications of the collector are as follows: the system incorporates a total of five flat-plate collectors, each with an individual dimension of 0.7 × 1 m.



ISSN 3030-3907




1-solar collector; 2, 15, 17, 18 three-way valves; 3-cold water tank; 4, 6, 7, 8 valves; 5- transfer of cold water; 9, 12, 14, 20 consumption meters; 10, 13, 19-circulation pumps; 11-tank-accumulator; 16-warm floor system; Filling and draining the circuit 21, 22 with water.

**Figure 1.2. The principle diagram of a warm floor system with a solar collector**

b) Tank-accumulator — serves to store the thermal energy collected by the solar collector and to distribute it to both the underfloor heating system and the domestic hot water supply. The tank consists of a galvanized cylindrical body, an external insulation layer, a serpentine heat-exchange coil, and instruments for monitoring temperature and pressure. The structural parameters of the accumulator tank are as follows: total capacity – 0.1 m³, diameter – 0.36 m, height – 1.0 m, internal coil pipe diameter – 0.02 m, with thermal insulation made of foam polystyrene, 20 mm thick.

c) Warm floor system — designed to heat indoor spaces through floor-based heat distribution. The system employs metal–polyethylene pipes arranged in a serpentine pattern. The pipe dimensions are 16 × 2 mm, with installation spacing options of 100, 150, 200, 250, and 300 mm. Depending on the spacing, the total pipeline length ranges between 32 m and 83 m.

The solar-assisted water-based floor heating system is organized into four operating circuits:

Circuit I — once the circuit is filled with water, valve 18 is opened and circulation pump 19 is activated. Water from the accumulator tank flows through consumption meter 20 and enters the flat-plate solar collector (1), where it is heated by solar energy. The heated water is then directed back to the accumulator tank



ISSN 3030-3907

(11) through valve 2. Continuous operation is maintained by the circulation pump, and control instruments record temperature and pressure values throughout the circuit.

Circuit II — after filling the system with water, valves 2, 15, 17, and 18 are opened, and circulation pump 19 is started. Water passes through consumption meter 20, enters the solar collector (1), and is heated to the required temperature. It is then directed through valve 2 and flow meter 14 (while circulation pump 13 remains idle) into the serpentine piping system (16) of the heated floor. As the water releases heat to the floor surface, it cools and returns to the solar collector, completing a continuous cycle until the desired floor temperature is achieved. Control devices monitor and record the system's temperature and pressure parameters.

Circuit III — when valves 15 and 17 are opened, water heated in the accumulator tank (11) is pumped into the floor heating pipeline via consumption meter 14 using circulation pump 13. The water transfers its heat to the floor surface and returns to the tank for reheating. This closed-loop process continues until the target floor temperature is achieved. Measurements of temperature and pressure are continuously recorded by the installed control devices.

Circuit IV — cold water is collected in a dedicated reservoir, after which pump 10 is activated. The flow is divided into two parts: one directed to the consumer as cold water, and the other sent to the accumulator tank (11) for heating. Both hot and cold water flow through meters 9 and 12, respectively. Depending on consumer demand, valves 7 and 8 are adjusted to mix the streams, thereby supplying hot water at the desired temperature.

Temperature variations at both the inlet and outlet of the underfloor heating circuit, as well as along the pipe length, are measured using a KSP-4 control device. Additional temperature readings in other system nodes are obtained via TR-100 thermoelectric thermometers and A43/A48 bimetallic thermometers. Water consumption in all circuits is monitored using LK-20 X(G) bucket meters, while a Testo 512 digital differential manometer is employed to measure pressure differences across the system nodes.

**Methodology of experimental research.** In this chapter of the dissertation, experimental investigations aimed at determining the hydraulic resistance and heat transfer performance of the underfloor heating system are conducted following the schematic configuration shown in Figure 1.2. The experimental determination of hydraulic resistance and heat transfer coefficients in laminar and turbulent flow regimes of water within the underfloor pipeline is performed in accordance with the established methodology outlined in [17].



ISSN 3030-3907

The procedure for conducting the experiments is as follows:

System preparation — the underfloor heating circuit is initially filled with water by opening valve 21, followed by opening valves 15 and 17. The working fluid is then heated to the required temperature either in the tank-accumulator or the solar collector. Once the desired temperature is achieved, circulation pump 13 is switched on, and water passes through consumption meter 14. The flow rate of hot water supplied to the test section is regulated using valves 17 and 15.

Flow regulation and measurements — depending on the investigated regime, the required velocity and volumetric flow rate of hot water are established. The hot water is circulated through the underfloor pipeline for a duration of five minutes. After stabilization, the specified flow rate is maintained consistently for an additional five minutes. During this period, the pressure drop is measured using a manometer, while inlet and outlet water temperatures are recorded with thermometers. This procedure is repeated for each experimental regime to ensure accuracy in determining hydraulic resistance and heat transfer coefficients.

System shutdown — upon completion of the measurements, circulation pump 13 is disconnected from the power supply. With valves 15 and 17 still open, valve 21 is opened to drain the system of water. Once the circuit is fully emptied, valves 15, 17, and 21 are closed, thereby concluding the experimental cycle.

**Experimental study of the hydrodynamic regime of a solar collector water heated floor system.** An experimental study of the hydrodynamic mode of the warm floor pipe was carried out according to the scheme shown in Figure 1.6. Experimental studies were carried out in the following range of main parameters: consumption of hot water: in laminar flow mode $G$=0,0043÷0,02 kg/sec, in the turbulent flow regime $G$=0,07÷0,093 kg/sec; average hot water temperature $t_c = 35 \dots 50$°C; average temperature on the floor surface $t_{floor} = 26$°C; the diameter of the pipe $d = 0{,}016\ m$; pipe placement step $s = 0{,}1\ m$, $s = 0{,}15\ m$, $s = 0{,}2\ m$, $s = 0{,}25\ m$, $s = 0{,}3\ m$; the speed of hot water in the underfloor heating pipe should not exceed 1 m/sec [18].

To determine the area of the laminar flow regime, it is necessary to calculate the value of the product $Gr \cdot Pr$ [19]:

$$Gr \cdot Pr = g\beta_г \frac{\Delta t d^3}{\nu_г^2} Pr_г \qquad (1.1)$$

where Gr-Grasgof number; Pr-Prandtl number; g-acceleration of free fall, m/s$^2$; $\beta$ -coefficient of volume expansion, 1/°C; Δt-temperature difference, °C; d-pipe inner diameter, m; $\nu$-kinematic viscosity coefficient, m/s2; index " г " indicates that the physical properties of liquids are obtained by temperature $t_г = 0{,}5(t_s + t_d)$.



ISSN 3030-3907

When $Gr \cdot Pr < 8 \cdot 10^5$, the flow regime is viscous. In the presence of heat exchange, the hydraulic resistance in smooth pipes in the viscous region of the laminar flow regime is defined as [20]:

$$\xi = \frac{64}{Re}\left(\frac{\mu_д}{\mu_c}\right)^n \quad (1.2)$$

here $n = C\left(Pe_1\frac{d}{l}\right)^m\left(\frac{\mu_д}{\mu_c}\right)^{-0,062}$; $Pe_1\frac{d}{l} = \frac{4G}{\pi l}\frac{c_p}{\lambda_c}$; $Pe_1\frac{d}{l} \le 1500$ when $C = 2,3$; $m = -0,3$; $Pe_1\frac{d}{l} \ge 1500$ when $C = 0,535$; $m = -0,1$ $Re$- Reynolds number.

When $Gr \cdot Pr > 8 \cdot 10^5$ the flow regime is viscous-gravitational. In the presence of heat exchange, the hydraulic resistance in smooth pipes in the viscous-gravitational field of the laminar flow regime is determined as follows [124]:

$$\xi = \frac{64}{Re}\left(\frac{Pr_d}{Pr_s}\right)^{1/3}\left[1 + 0,22\left(\frac{GrPr}{Re}\right)^{0,15}\right] \quad (1.3)$$

In the presence of heat exchange, the hydraulic resistance in the turbulent flow regime is defined as [21]:

$$\xi = \frac{0,3164}{Re^{0,25}}\left(\frac{Pr_d}{Pr_s}\right)^{1/3} \quad (1.4)$$

The total pressure loss in a water-heated floor node is equal to the sum of the linear pressure loss and the pressure loss overcoming local resistances [21]:

$$\Delta p_у = \Delta p_ч + \Delta p_м \quad (1.5)$$

Linear pressure loss in a water-heated floor pipe [21]:

$$\Delta p_ч = \xi\frac{\rho w^2}{2}\frac{d}{l} \quad (1.6)$$

here $\rho$- density of hot water, kg/m$^3$; $w$- the speed of hot water in the pipe, m/s; $d$- inner diameter of the pipe, m; $l$- the total length of the pipe, m.

Pressure loss to overcome local resistances in a water-heated floor pipe [21]:

$$\Delta p_m = \sum\xi\frac{\rho w^2}{2} \quad (1.7)$$

here $\sum\xi$- sum of local (all bends ("elbow")) resistances at the node.

The pump power required to drive the hot water passing through the water warm floor pipe is determined by the following formula [21]:

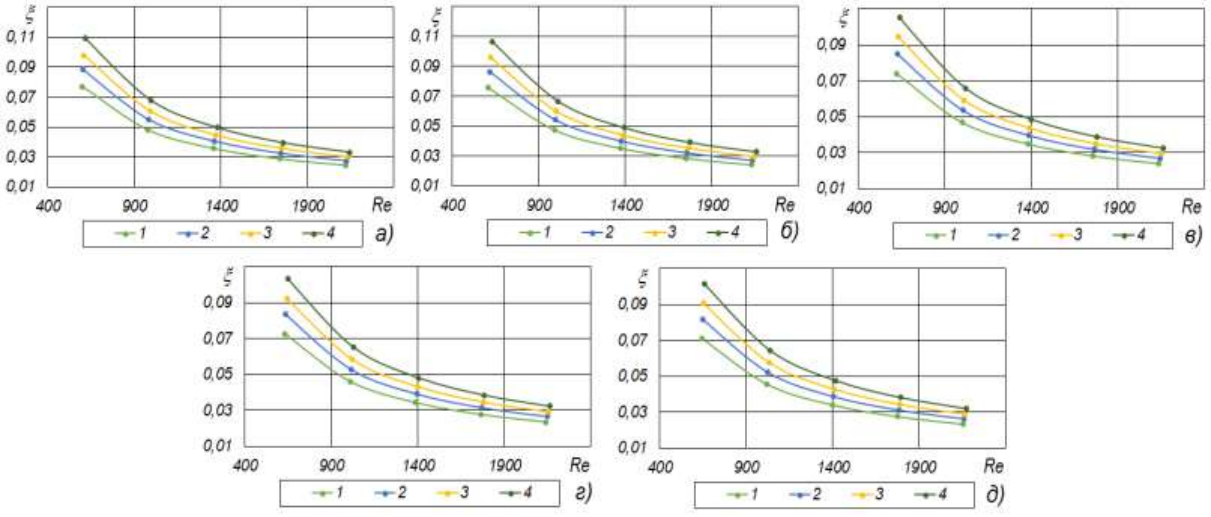
$$N = \frac{G\Delta p_у}{\rho\eta} \quad (1.8)$$

here $G$- consumption of hot water, kg/sec; $\eta$- Pump Efficiency, usually $\eta$=0,7.

**Laminar flow mode.** Experimental results on the coefficient of hydraulic resistance of the pipe in the laminar flow mode of hot water at different location steps of the warm floor pipe and at different temperatures of hot water are presented in Figure 1.3, and the experimental results on pressure loss and pump power are presented.



ISSN 3030-3907




a-s=100 mm; b-s=150 mm; v-s=200 mm; g-s=250 mm; d-s=300 mm;
1-$t_{water}$ = 35℃; 2-$t_{water}$ = 40℃; 3-$t_{water}$ = 45℃; 4-$t_{water}$ = 50℃

**Figure 1.3. Graphs of changes in the coefficient of hydraulic resistance in the laminar flow mode depending on the placement step of the warm floor pipe and the hot water temperature**

The analysis of the results of the hydraulic resistance coefficient presented in Figure 1.3 shows that the hydraulic resistance coefficient of the warm floor pipe is significantly dependent on the pipe layout step and the hot water temperature, and the hydraulic resistance coefficient increases as the pipe layout step decreases and the hot water temperature increases. According to the experimental results, the coefficient of hydraulic resistance is 0.024...0.109 when the positioning step is 100 mm in laminar flow mode, 0.024...0.107 when it is 150 mm, 0.024...0.105 when it is 200 mm, 0.024...0.103 when it is 250 mm, when it is 300 mm It was determined to vary between 0.024...0.101.

The experimental results obtained on hydraulic resistance in the laminar flow mode were processed and the following empirical relationships were obtained at different placement steps of the pipe:

$s = 100\ mm$ when:

$$\xi = \frac{20{,}967}{Re^{0{,}924}}\left(\frac{Pr_d}{Pr_s}\right)^{1{,}037}\left(\frac{GrPr}{Re}\right)^{0{,}012} \quad (1.9)$$

$s = 150\ mm$ when:

$$\xi = \frac{20{,}843}{Re^{0{,}926}}\left(\frac{Pr_d}{Pr_s}\right)^{1{,}035}\left(\frac{GrPr}{Re}\right)^{0{,}014} \quad (1.10)$$

$s = 200\ mm$ when:

$$\xi = \frac{21{,}023}{Re^{0{,}928}}\left(\frac{Pr_д}{Pr_c}\right)^{1{,}037}\left(\frac{GrPr}{Re}\right)^{0{,}014} \quad (1.11)$$

$s = 250\ mm$ when:



ISSN 3030-3907

$$\xi = \frac{21{,}299}{Re^{0{,}931}} \left(\frac{Pr_d}{Pr_s}\right)^{1{,}040} \left(\frac{GrPr}{Re}\right)^{0{,}014} \quad (1.12)$$

$s = 300\ mm$ when:

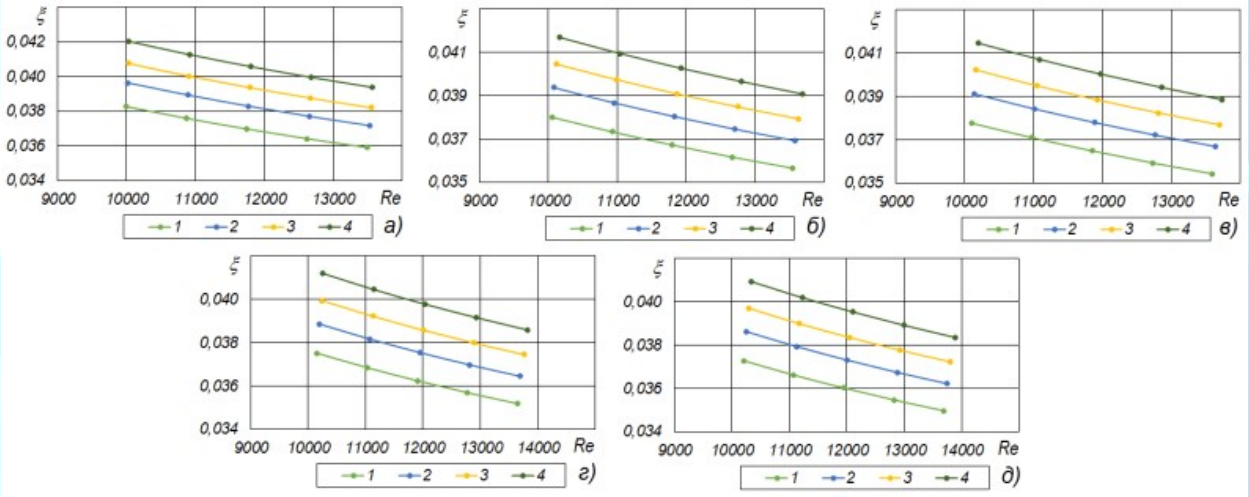
$$\xi = \frac{21{,}347}{Re^{0{,}933}} \left(\frac{Pr_d}{Pr_s}\right)^{1{,}040} \left(\frac{GrPr}{Re}\right)^{0{,}015} \quad (1.13)$$

In the generalized case, the following equation was obtained:

$$\xi = \frac{20{,}44}{Re^{0{,}929} s^{0{,}018}} \left(\frac{Pr_d}{Pr_s}\right)^{1{,}038} \left(\frac{GrPr}{Re}\right)^{0{,}014} \quad (1.14)$$

The obtained relation (1.14). $400<Re<2200$, $1{,}25<Pr_d/Pr_s<1{,}71$, $9{,}7\cdot10^5<GrPr<34\cdot10^5$ appropriate at intervals. Calculation error ±2%.

**Turbulent flow mode.** Experimental results on the coefficient of hydraulic resistance of the hot water pipe in the turbulent flow regime of the warm floor pipe at different location steps and at different hot water temperatures are shown in Figure 1.4, and the experimental results on pressure loss and pumping power are presented.




а-s=100 mm; б-s=150 mm; в-s=200 mm; г-s=250 mm; д-s=300 mm;
1-$t_{water}$ = 35°C; 2-$t_{water}$ = 40°C; 3-$t_{water}$ = 45°C; 4-$t_{water}$ = 50°C

**Figure 1.4. Variation of the coefficient of hydraulic resistance in the turbulent flow regime depending on the placement step of the warm floor pipe and the temperature of the hot water**

The analysis of the results of the hydraulic resistance coefficient presented in Figure 1.4 shows that the hydraulic resistance coefficient of the warm floor pipe is significantly dependent on the pipe layout step and the hot water temperature, and the hydraulic resistance coefficient increases as the pipe layout step decreases and the hot water temperature increases. According to the experimental results, the hydraulic resistance coefficient is 0.036...0.042 when the placement step is 100 mm in the turbulent flow mode, 0.035...0.41 when it is 150 mm, 0.034...0.040 when it is 200 mm, 0.033...0.039 when it is 250 mm, 300 mm, it was found to change in the range of 0.032...0.038.



ISSN 3030-3907

The experimental results obtained on the hydraulic resistance in the turbulent flow mode were processed and the following empirical correlations were obtained at different placement steps of the pipe.:

$s = 100\ mm$ when:

$$\xi = \frac{0{,}258}{Re^{0{,}214}}\left(\frac{Pr_d}{Pr_s}\right)^{0{,}295} \quad (1.15)$$

$s = 150\ mm$ when:

$$\xi = \frac{0{,}259}{Re^{0{,}215}}\left(\frac{Pr_d}{Pr_s}\right)^{0{,}297} \quad (1.16)$$

$s = 200\ mm$ when:

$$\xi = \frac{0{,}26}{Re^{0{,}216}}\left(\frac{Pr_d}{Pr_s}\right)^{0{,}298} \quad (1.17)$$

$s = 250\ mm$ when:

$$\xi = \frac{0{,}262}{Re^{0{,}218}}\left(\frac{Pr_d}{Pr_s}\right)^{0{,}3} \quad (1.18)$$

$s = 300\ mm$ when:

$$\xi = \frac{0{,}263}{Re^{0{,}219}}\left(\frac{Pr_d}{Pr_s}\right)^{0{,}301} \quad (1.19)$$

In the generalized case, the following equation was obtained:

$$\xi = \frac{0{,}252}{Re^{0{,}217}s^{0{,}019}}\left(\frac{Pr_д}{Pr_c}\right)^{0{,}298} \quad (1.20)$$

Equation (1.20) derived from the above equations $10000<Re<14000$, $1{,}25<Pr_d/Pr_s<1{,}71$ appropriate at intervals. Calculation error ±2%.

**Assessment of adequacy of theoretical and experimental results of hydrodynamic research.** Adequacy was assessed by Fisher's criterion [22]:

$$F_{cal} = \frac{S^2_{ад}}{S^2_y} \quad (1.21)$$

where $S_{ad}$ -is the adequacy dispersion of the models; $S_y$ - is the variance of mutual proximity of $y$ quantities

Adequacy variance:

$$S^2_{ad} = \frac{\sum_{i=1}^{n}(y-\hat{y})^2}{f_1} \quad (1.22)$$

where $y$ - is a theoretical function; $\hat{y}$ - is the desired function; $f_1$ -is the number of degrees of freedom.

Mutual proximity variance:

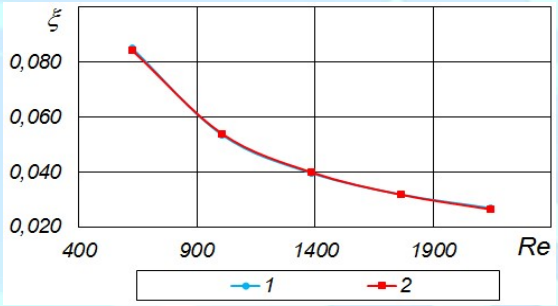
$$S^2_y = \frac{\sum_{i=1}^{n}(y-\bar{y})^2}{n-1} \quad (1.23)$$

here $\bar{y}$ – $y$ Arithmetic mean value of; $n$ – number of observations.

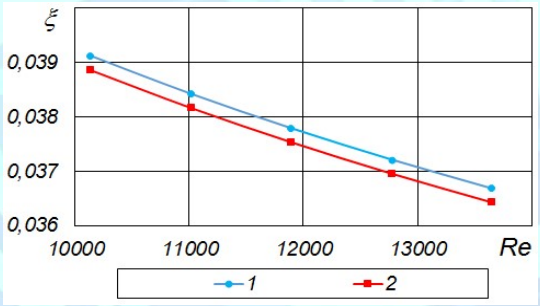


ISSN 3030-3907

Figure 1.5 shows a comparison of the theoretical and experimental results obtained for the determination of hydraulic resistance in laminar and turbulent flow regimes in a pipe.




1-theoretical (formula 1.3) results; Results of experiment 2 (formula 1.14).




1-theoretical (formula 1.4) results; Results of experiment 2 (formula 1.20).

**Figure 1.5. Comparison of theoretical and experimental results obtained on hydraulic resistance in laminar and turbulent flow regimes**

Confidence Probability from Table of Fisher's Criterion Values P=0,99, degrees of freedom $f_1 = 95$ and number of observations $n = 99$ suitable for the case $F_{table} = 0{,}62$ we find the value. Calculated value of the Fisher criterion for the formula (1.14). $F_{calculation} = 0{,}3$. Calculated value of the Fisher criterion for the formula (1.20). $F_{calculation} = 0{,}13$. It can be seen that in both cases $F_{cal} < F_{table}$, so the model is adequate. Empirical correlations obtained for determining the hydraulic resistance in warm floor pipes are fully adequate with the experimental results, and they can be used to evaluate the hydrodynamic efficiency of the warm floor system with solar collectors in different flow regimes of hot water.

**Conclusion.** Effect of hot water temperature and pipe spacing on hydraulic resistance, pressure loss, and pump power

Experimental investigations were conducted to determine the influence of hot water temperature and pipe installation pitch on the hydraulic resistance coefficient, pressure losses, and pump power under laminar and turbulent flow regimes.

In laminar flow conditions, with water temperatures ranging from 35–50 °C and pipe spacing between 0.1–0.3 m, the hydraulic resistance coefficient was found to vary within the range of 0.024–0.109. The corresponding pressure losses were measured between 55–612 Pa, while pump power requirements ranged from 1–17 W.

In turbulent flow conditions, at the same temperature and pipe spacing ranges, the hydraulic resistance coefficient was recorded within 0.032–0.042.



ISSN 3030-3907

Pressure losses significantly increased to values between 5506–36733 Pa, and pump power varied within 6–65 W.

Effect of hot water temperature and pipe spacing on heat transfer performance

The impact of hot water temperature and pipe pitch on the overall heat transfer coefficient, convective heat transfer rate, and the total amount of transferred heat was also experimentally assessed.

In the laminar regime, the heat transfer coefficient was observed in the range of 0.82–2.35, with convective heat flux values between 33–92 W/(m²·°C). The total heat transfer capacity of the system under these conditions ranged from 835–5438 W.

In the turbulent regime, the heat transfer coefficient increased substantially, ranging from 49–78. Convective heat flux reached values between 1973–3089 W/(m²·°C), while the total heat transfer capacity varied between 52883–251348 W.

## REFERENCES

1. K. Yu, Y. Tan, T. Zhang, J. Zhang, X. Wang, The traditional Chinese kang and its improvement: A review, Energy Build. 218 (2020) 110051, https://doi.org/10.1016/j.enbuild.2020.110051.

2. Z. Zhuang, Y. Li, B. Chen, J. Guo, Chinese kang as a domestic heating system in rural northern China–A review, Energy Build. 41 (1) (2009) 111–119.

3. D. Wang, R. Zhang, Y. Liu, X. Zhang, J. Fan, Optimization of the flow resistance characteristics of the direct return flat plate solar collector field, Sol. Energy 215 (2021) 388–402.

4. S. Paraschiv, N. BˇarbuЯtˇa-MisЯu, L.S. Paraschiv, Technical and economic analysis of a solar air heating system integration in a residential building wall to increase energy efficiency by solar heat gain and thermal insulation, Energy Reports, S 6 (2020) 459–474.

5. H. Esen, M. Esen, O. Ozsolak, Modelling and experimental performance analysis of solar-assisted ground source heat pump system, J. Exp. Theor. Artif. Intell. 29 (1) (2017) 1–17.

6. Uzakov G.N., Khamraev S.I., Khuzhakulov S.M. Rural house heat supply system based on solar energy // IOP Conf. Series: Materials Science and Engineering 1030 (2021) 012167 IOP Publishing doi:10.1088/1757-899X/1030/1/012167.

7. M. Esen, T. Ayhan, Development of a model compatible with solar assisted cylindrical energy storage tank and variation of stored energy with time for different phase change materials, Energy Convers. Manage 37 (12) (1996) 1775–1785.



ISSN 3030-3907

8. M. Esen, A. DurmusЯ, A. Geometric design of solar-aided latent heat store depending on various parameters and phase change materials, Sol.Energy 62 (1998) 19–28.
9. Y. Liu, T. Li, C. Song, D. Wang, J. Liu, Field study of different thermal requirements based on the indoor activities patterns of rural residents in winter in Northwest China, Science and Technology for the, Built Environment 24 (8) (2018) 867–877.
10. Y.Y. Wang, W.J. Kang, Y.F. Liu, R. Huang, J.P. Liu, A heating strategy for rural residential buildings based on behavior patterns of residents in shaanxi province, Acta energiae solaris sinica 39 (2018) 3026–3031 (In chinese).
11. Низовцев М.И., Сахаров И.А. Определение тепловых и конструктивных параметров водяного теплового пола // Научно-практическая конференция “Энерго-и ресурсоэффективность малотэтажных жилых зданий”. Институт теплофизики С.С. Кутателадзе СО РАН, 19-20 марта 2013 г. – с. 39-42.
12. Bearzi V. Теплые полы. Теория и практика // АВОК. – 2005. №7. – с. 70-82.
13. Почему водяной теплый пол, а не электрический. ООО «ВАНТУБО-СЕРВИС» [Электронный ресурс] URL: http://www.vantubo-service.ru/neelectro.
14. СНиП 41-01-2003. «Отопление, вентиляции и кондиционирование».
15. ГОСТ 13732-2-2008. «Эргономика термальной среды. Методы оценки реакции человека при контакте с поверхностями. Часть2. Контакт с поверхностью умеренной температуры».
16. Хамраев С.И., Хужакулов С.М., Камолов Б.И. Қуёш иссиқлик таъминоти тизимли тажриба қишлоқ уйининг иссиқлик балансини тадқиқот қилиш. // «Энергия ва ресурс тежаш муаммолари». Тошкент, 2021. № 3, 181-191-б.
17. Руководство к практическим занятиям в лаборатории процессов и аппаратов химической технологии: Учебное пособие для вузов. / Под ред. П.Г. Романкова. – Л.: Химия, 1990. – 272 с.
18. Водяной теплый пол. Проектирование, монтаж, настройка. 2020. www.valtek.ru.
19. Краснащеков Е.А., Сукомел А.С. Задачник по теплопередаче: Учебное пособие для вузов. – М.: Энергия, 1980. – 288 с.
20. Каневец Г.Е. Обобщенные методы расчета теплообменников. – Киев: Наук, думка, 1979, - 352 с.
21. Михеев М.А., Михеева И.М. Основы теплопередачи. Изд. 2-е. М.: Энергия, 1977. – 344 с.



ISSN 3030-3907

22. Бабин А.В., Ракипов Д.В. Организация и математическое планирование эксперимента. Екатеринбург, уральский Федеральный Университет, 2014. – 113 с.
23. L. A. Aliyarova, U. H. Ibragimov,, S. I. Khamraev. Investigation of hydrodynamic processes in tubes of a combined solar collector. AIP Conference Proceedings 2612, 030018 (2023); https://doi.org/10.1063/5.0124758
24. Uzakov G. N., Charvinski V. L., Ibragimov U. Kh., Khamraev S. I., Kamolov B. I. (2022) Mathematical Modeling of the Combined Heat Supply System of a Solar House. Energetika. Proc. CIS Higher Educ. Inst. and Power Eng. Assoc. 65 (5), 412–421. https://doi.org/10. 21122/1029-7448-2022-65-5-412-421
25. Sh Mirzaev, J Kodirov, S I Khamraev. Method for determining the sizes of structural elements and semi-empirical formula of thermal characteristics of solar dryers// APEC-V-2022 IOP Conf. Series: Earth and Environmental Science IOP Conf. Series: Earth and Environmental Science 1070(2022) 012021 IOP Publishing doi:10.1088/1755-1315/1070/1/012021.
26. S I Khamraev. Study of the combined solar heating system of residential houses. BIO Web of Conferences 71, 02017 (2023) https://doi.org/10.1051/bioconf/20237102017 CIBTA-II-2023
27. Saydullo Khuzhakulov, Zokir Pardaev, Sardor Khamraev. Thermal conditions of systems for solar thermal regeneration of adsorbents // IPICSE 2020 IOP Conf. Series: Materials Science and Engineering 1030 (2021) 012166 IOP Publishing doi:10.1088/1757-899X/1030/1/012166



ISSN 3030-3907